Three-dimensional microscale simulation of colloidal particle transport and deposition in model porous media with converging/diverging geometries

Yajie Li[a,b], Azita Ahmadi[b,*], Aziz Omari[c], Hongting Pu[a]

[a] School of Materials Science & Engineering, Tongji University, Shanghai, 201804, China
[b] I2M, Arts et Métiers Paris-Tech, CNRS, Esplanade des Arts et Métiers, 33405 Talence Cedex, France
[c] I2M, Bordeaux-INP, CNRS, Esplanade des Arts et Métiers, 33405 Talence Cedex, France

GRAPHICAL ABSTRACT

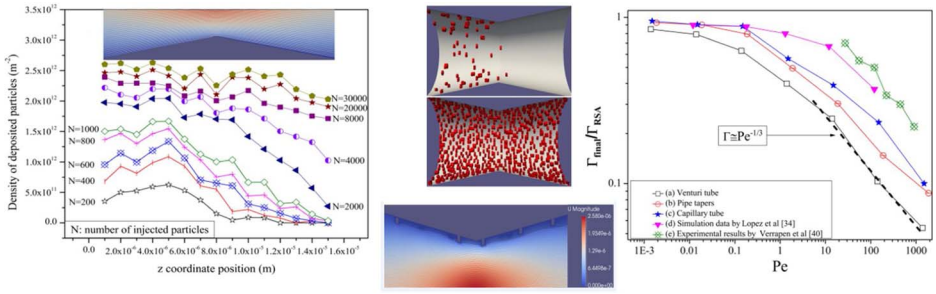

ARTICLE INFO

Keywords:
3D-PTPO (three-dimensional particle tracking model by python® and OpenFOAM®)
Microscale simulation
Converging/diverging pipes
Spatial density distribution
Surface coverage
Péclet number

ABSTRACT

The microscale simulation of colloidal particle transport and deposition in porous media was achieved with a novel colloidal particle tracking model, called 3D-PTPO (Three-Dimensional Particle Tracking model by Python® and OpenFOAM®), using a Lagrangian method. Simulations were performed by considering the elementary pore structure as a capillary tube with converging/diverging geometries (tapered pipe and venturi tube). The particles are considered as a mass point during transport in the flow and their volume is reconstructed when they are deposited. The main feature of this novel model is to renew the flow field by reconstructing the pore structure by taking the volume of the deposited particles into account. The influence of the particle Péclet number (Pe) and the pore shape on the particle deposition therein is investigated. The results are analyzed in terms of deposition probability and dimensionless surface coverage as a function of the number of injected particles for a vast range of Péclet numbers thus allowing distinguishing the behavior in diffusion dominant and advection dominant regimes. Finally, the maximum dimensionless surface coverage $\Gamma_{final}/\Gamma_{RSA}$ is studied as a function of Pe. The declining trend observed for high Pe is in good agreement with experimental and simulation results found in the literature.

1. Introduction

Transport and deposition of colloidal particles in porous media under flow is encountered in a wide range of environmental and industrial applications including aquifer remediation [1], fouling of surfaces [2], therapeutic drug delivery [3,4], catalytic processes carried out through filter beds [5,6] and drinking water treatment [7]. The investigation of colloid transport and deposition processes in porous media has therefore drawn considerable attention during the last decades. Focuses on particular mechanisms among all those generally

* Corresponding author at: I2M-TREFLE, UMR CNRS, Arts et Métiers Paris-Tech, Esplanade des Arts et Métiers, 33405 Talence Cedex, France.
E-mail address: azita.ahmadi-senichault@u-bordeaux.fr (A. Ahmadi).

involved in such processes have been the subject of research works in the literature [8–13]. The most realistic representation of a porous medium is as a collection of solid grains, each being considered as a collector. The process of particle deposition is, therefore, divided into two steps: transport to the collector and deposition due to short-range particle/collector physico-chemical interactions. Such interactions are represented through a potential function usually obtained from the DLVO theory that includes electrostatic, van der Waals, and short range Born repulsion forces [7,14]. If particles and collectors are similarly charged and salt is low, the interaction potential contains two minima and one energy barrier making deposition condition unfavorable. When the salt concentration is very high or when particles and collectors are of opposite charges, the potential is purely attractive, leading to favorable deposition [15].

To experimentally investigate colloids deposition mechanisms, impinging jet flow or parallel-plate cells are commonly used because of simplicity of flow structure and are coupled to various techniques such as direct observation techniques [16–19]. In porous media, column experiments using native or fluorescent polystyrene Latex particles are the most commonly performed owing to their simplicity giving output data in the form of Breakthrough curves (BTC) [20]. These are sometimes coupled to other techniques as gamma-ray attenuation [21–23], magnetic resonance imaging [24], laser scanning cytometry [25], microscopy and image processing [26,27].

In column experiments, the BTC encompass all involved sorts of particle-particle and particle-collector interactions. To interpret experimental data, an Eulerian approach may be adopted consisting in solving the advection-dispersion equation containing one or two source terms representing adsorption and desorption isotherms [28].

Risbud and Drazer [29] have considered the case of non-Brownian particles moving past a spherical or a cylindrical collector in Stokes regime by focusing on the distribution of particles around the obstacle and the minimum particle-obstacle distance attained during particle motion. They show that very small surface-to-surface separation distances would be common during the motion highlighting that short-range non-hydrodynamic interactions may have a great impact during particle motion.

Unni and Yang [18] have experimentally investigated colloid deposition in a parallel-plate flow cell by means of direct videomicroscopic observation. They focused on the influence of the flow's Reynolds number, physico-chemical conditions and particle size on surface coverage. To simulate deposition therein, the Langevin equation, particle-particle and particle-wall hydrodynamic interactions together with the DLVO theory were used. Accordance between experimental and simulation results were observed for flow Reynolds numbers scanned between 20 and 60.

In filtration processes, the porous medium is usually assumed to be composed of unit bed elements each containing a given number of unit cells whose shape is cylindrical with constant or varying cross sections. Chang et al. [30] have used Brownian dynamic simulation to investigate deposition of Brownian particles in model parabolic constricted tubes, hyperbolic constricted tubes and sinusoidal constricted tubes. Here again Langevin equation with corrected hydrodynamic particle/wall interactions and DLVO interaction were solved to get particles trajectories. Therefore the single collector efficiency that describes the initial deposition rate was evaluated for every geometry at various Reynolds numbers.

A more realistic porous geometry for the study of transport and deposition is a bed of packed collectors of a given shape. Boccardo et al. [31] have numerically investigated deposition of colloidal particles under favorable conditions in 2D porous media composed of grains of regular and irregular shapes by solving the Navier-Stokes equations together with the advection-dispersion equation. Then and even if particles trajectories can't be specified, it was possible to determine how neighboring grains mutually influence their collection rates. They show that the Brownian attachment efficiency deviates appreciably from the case of single collector. Similarly Coutelieris et al. [32] have considered flow and deposition in a stochastically constructed 3D spherical grain assemblage by focusing on the dependence of capture efficiency at low to moderate Péclet numbers and found that the well-known sphere-in-cell model remains applicable provided that the right porous medium properties are taken into account. Nevertheless the scanned porosities were too close to unity to be representative of actual porous media. In their work, Lagrangian approach is used to track particle displacement in 3D packed beds allowing to study microscale transport and deposition of colloidal particles. For that purpose Lattice Boltzmann techniques are used for calculating hydrodynamic and Brownian forces acting on moving particles with local evaluation of physico-chemical interaction potential showing the hydrodynamic retardation to reduce the kinetics of deposition in the secondary minimum under unfavorable conditions [32] and particles retention in flow vortices [33].

In most of these simulation approaches the characteristic size of the flow domain is many orders of magnitude greater than the particle size so that the jamming ratio (the ratio of characteristic size of flow domain to the particle size) is high enough to consider that the initial flow domain remains unaffected by particle deposition. For many systems however the jamming ratio may be low and thought straining phenomenon is negligible, colloids deposition should greatly impact the flow structure and strength and therefore the particle deposition process. In the present paper we focus on such impact and will simulate colloids deposition in porous media under favorable deposition condition by adopting the unit bed approach where the unit cell is a constricted tube with two converging-diverging forms, i.e.: tapered pipe and venturi-like tube. To balance the inherent rising of simulation cost, we will restrict this study to dilute colloidal suspensions where hydrodynamic interactions between flowing particles are negligible and will adopt a simple approach that is detailed hereafter and a novel 3D-PTPO (Three-Dimensional Particle Tracking model by Python® and OpenFOAM®) code developed in our laboratory. We will mainly focuses on deposition probability, the spatial distribution of deposited particles and surface coverage as functions of flow strength through the particle Péclet number (see Section 2.2 for definition). The simulation method and considered conditions are described in details in Section 2 and obtained results are presented and discussed in Section 3. The main conclusions are then drawn in Section 4.

2. Numerical simulations

Porous media are often considered as a bundle of capillaries, therefore when particle transport and deposition has been simulated in one capillary, the process in the whole porous media could be predicted with suitable imposed boundary conditions between capillaries [4]. The simplest model consist in representing the porous medium as a series of parallel capillaries of circular cross section whose mean radius is given by $\sqrt{(8k/\varepsilon)}$ where k and ε are the porous medium permeability and porosity respectively. As this is a crude representation of the pore geometry, in the present work, we deal with three-dimensional numerical modeling of the process of transport and deposition of particles in capillaries with converging/diverging geometries (Fig. 1) that are believed to be more realistic pore shapes. The two pore geometries considered have a length of 15 μm, a volume of 753 μm^3, and the pore body radius (R_B) to pore throat radius (R_T) ratio is chosen to be 1.5 [35]. The transported particles have a radius, a_p, of 0.2 μm.

A sensitivity analysis was undertaken to explore the effect of mesh numbers on the accuracy of our results by varying the number of grid block used for the numerical simulations. The analysis was first based on the flow field for both types of capillary tubes before any particle deposit. Moreover, the deposition probability and distribution of deposited particles are compared for various mesh numbers going from 80,000 to 160,000. The results indicate that 80,000 grid blocks are sufficient for our computations.

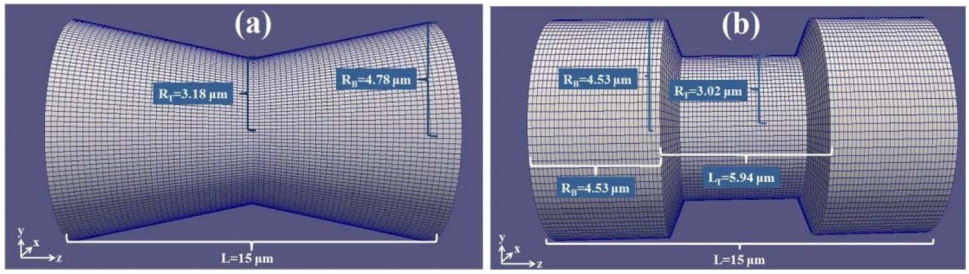

Fig. 1. Geometry and meshing of the two configurations considered: (a) tapered pipe; (b) venturi tube.

2.1. Hypothesis of the problem

In the present work the following assumptions are adopted:

(1) The fluid is Newtonian and incompressible and the flow is creeping.
(2) The particle Reynolds number defined as $Re = \rho \bar{u} a_p/\mu$ (where ρ and μ are the fluid density and dynamic viscosity, a_p the particle radius and $\bar{u}$ the mean velocity at the pore throat under clean bed conditions) is small. The flow is therefore considered laminar and non-inertial (creeping).
(3) The scale of the variation of the flow velocity over a_p is small compared to the maximum velocity. We can therefore reasonably assume that the particle transported by the flow is a mass point.
(4) The particle-pore wall physico-chemical interaction is considered purely attractive and the particle-particle interaction purely repulsive.
(5) Deposition is irreversible and both hydrodynamic and physico-chemical removal of deposited particles is prohibited.

2.2. Governing equations and boundary conditions

The governing equations for the creeping flow of an incompressible Newtonian fluid are the Stokes equations given by:

$$0 = -\nabla p + \mu \nabla^2 \mathbf{v} \tag{1}$$

$$\nabla \cdot \mathbf{v} = 0 \tag{2}$$

where p is the pressure and **v** stands for the flow velocity.

The no-slip boundary condition is applied on the pore wall and on the interface between the fluid and a deposited particle. At the inlet, the pressure is set to a fixed value, while at the outlet it is set to zero. In order to fulfill the requirement of creeping flow and to investigate a large range of Péclet numbers, the pressure at the inlet will be varied between 10^{-5} and 10 Pa. The Péclet number is defined as:

$$Pe = \frac{\bar{u}\, a_p}{D} \tag{3}$$

where *D* is the bulk diffusion coefficient of the particles in the fluid.

2.3. Methodology and tools

Since the incoming suspension is considered to be dilute, particles are injected individually, randomly and sequentially at the inlet of the geometry [34] and a Lagrangian method is used to track the trajectories of the colloidal particles. Once the injected particle is deposited onto the surface wall or leaves the domain, another particle is injected and the whole process will be repeated until the pre-defined cut-off value of deposition probability (2%) is reached. The deposition probability is defined as the ratio of the number of deposited particles over the number of injected particles.

Simulations are carried out by the 3D-PTPO code, coupling OpenFOAM® (Open Field Operation and Manipulation) and Python®. Firstly, the flow field is computed using OpenFOAM® software. Secondly, the injected particles are tracked using a code developed using Python®, which is an open source programming language used for both standalone programs and scripting applications in a wide variety of domains.

The detailed steps of the 3D-PTPO code is as following: the calculated flow field (CSV format) is obtained after solving the equation of motion, then a particle is injected at the entrance plane (z = 0) with the initial coordinates (x,y) generated by two independent pseudo-random series [34]. Afterwards, a loop is carried out to track the movement of the particle in the flow domain. For that purpose, the particle velocity **V** at every position within the domain is calculated by the vector summation of the advection velocity $\mathbf{V_{conv}}$ and the Brownian diffusion velocity $\mathbf{V_{diff}}$. $\mathbf{V_{conv}}$ is obtained from OpenFOAM® by interpolating the velocity of the nearest eight mesh-nodes surrounding the particle. $\mathbf{V_{diff}}$ represents the random velocity of the particle due to Brownian motion at every time-step, given by:

$$\mathbf{V_{diff}} = \|\mathbf{V_{diff}}\|(\alpha\, \mathbf{i} + \beta\, \mathbf{j} + \gamma\, \mathbf{k})$$

$$\alpha = \frac{a}{\sqrt{a^2+b^2+c^2}};\ \beta = \frac{b}{\sqrt{a^2+b^2+c^2}};\ \gamma = \frac{c}{\sqrt{a^2+b^2+c^2}}$$

$$\|\mathbf{V_{diff}}\| = \sqrt{\frac{D}{\mathrm{tr}}} = \sqrt{\frac{kT}{6\pi\mu a p \mathrm{tr}}} \tag{4}$$

where a, b and c are random numbers between -1 and 1; α, β and γ are determined by the normalization of the three random numbers, thus giving a unit vector with a random direction $\alpha\mathbf{i} + \beta\mathbf{j} + \gamma\boldsymbol{k}$, k_B is the Boltzmann constant and T is the absolute temperature. The parameters used in the simulation are summarized in Table 1. Here we neglect the particles' mobility reduction near the wall that decreases the particle's diffusivity. Indeed, the explicit evaluation of this reduction is of no practical interest in this work since we do not calculate hydrodynamic forces acting on a physical particle moving near the wall albeit one could have advocated a phenomenological correction of the diffusivity coefficient as particles approach the wall. This has not been done in this work where D is considered constant. In this study, the reference time t_r, is defined as [34]:

$$t_r = \zeta/(2\, u_{max}) \tag{5}$$

max

The position of a moving particle is obtained by summing the old position vector $\mathbf{X_{old}}$ and the updated velocity multiplied by the reference time t_r:

$$X_{new} = X_{old} + V \times t_r \tag{6}$$

Table 1
Parameters used for simulations.

Parameters	Values
Particle radius, a_p (m)	2×10^{-7}
Length of the pipes, L (m)	1.5×10^{-5}
Boltzmann constant, k_B (J/K)	1.38×10^{-23}
Temperature, T (K)	293.15
Dynamic viscosity, μ (Pa·s)	10^{-3}

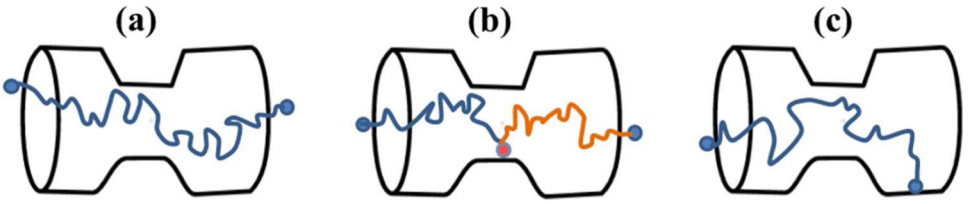

Fig. 2. Sketches of possible particle trajectories: (a) flow through; (b) approaching a deposited particle (in blue) and bouncing back to the bulk flow (in red); (c) deposited on the wall. (For interpretation of the references to colour in this figure legend, the reader is referred to the web version of this article).

During the particle tracking process, three situations may occur: (1) the particle leaves the domain without deposition (Fig. 2a); (2) the center-to-center distance between the moving particle and any other particle already deposited is less than a predefined value, the transported particle will bounce back to the bulk flow, and the tracking process will continue, (Fig. 2b); (3) the particle approaches the pore wall and will be deposited if enough free surface is available for deposition (Fig. 2c). In that case, the meshes containing the reconstructed deposited particle are considered as solid to take the particle's volume into account, and the flow field is then recalculated. As soon as the loop for one particle finishes, another particle is injected. The injection process is repeated until the particle deposition probability defined as the ratio of the number of deposited particles over the number of injected particles, reaches a minimum value of 2%.

It must be noted that in order to ensure feasible numerical computations in terms of meshing and therefore computation time, the volume of the deposited particle reconstructed is not spherical. Indeed, in case of a spherical particle, a correct representation of the particle/wall contact point for flow computation would require an extremely fine meshing and would hinder the feasibility of this work which has required a great number of simulations. Therefore, once deposited the reconstructed particle is a circle based cylinder in contact with the pore-wall by its base.

3. Results and discussion

For each geometry, simulations with different Péclet numbers ranging typically from 10^{-3} to 10^{3} were carried out to investigate the influence of the flow regime on particle's deposition probability, the spatial density distribution of the deposit and the surface coverage. For low Pe (Pe $<<$ 1), the particle movement is dominated by the diffusion mechanism, while for high Pe (Pe $>>$ 1), the particle's transport is governed by advection.

3.1. Deposition probability

The deposition probability is defined as the ratio of the number of deposited particles over the number of injected particles and is calculated over groups of 200 particles for each simulation. This was done for each geometry and since obtained results are almost similar, only those corresponding to the tapered pipe are presented for clarity. The evolution of the deposition probability versus the number of injected particles (N) at different Pe is plotted in Fig. 3 in case of tapered pipe. For the advection-dominant regime corresponding to high Péclet numbers, the value of the deposition probability is relatively small. This is due to, on one hand, the low residence time of the particles in the domain, as the advection velocity is high and to the hydrodynamic shadowing effect, on the other hand that leads to larger exclusion surfaces compared to the diffusion dominant regime and therefore smaller areas are available for deposition around the already deposited particles. These exclusion zones are more extended downstream of deposited particles and increase both in size and shape complexity as Pe increases. For low Péclet numbers, the deposition probability is relatively high and exhibits a plateau at the early stages of the injection process. This is due to the fact that compared to the high Péclet regime, the exclusion area at low Pe ($4\pi a_p^2$, for deposition of non-interacting spheres on a flat surface in purely diffusive regime) is smaller and the

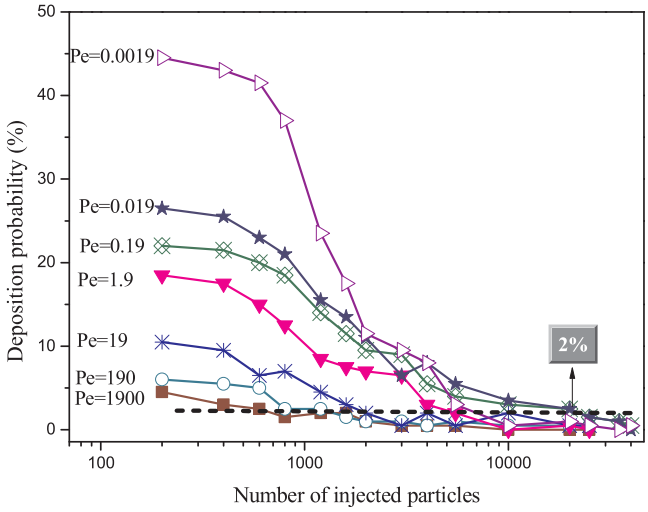

Fig. 3. Variation of deposition probability versus N at different Pe for the tapered pipe.

pore-wall surface is available to a large extent for the injected particles to deposit on. However and strictly speaking, in evaluating the extent of the exclusion area due to blocking effect one should in general take into account not only steric interaction but also the extra contribution of DLVO origin [36–38]. In this work only steric contribution has been considered. Moreover due to shortness of the pore length and still low residence time of flowing particles in the pore space, the maximum deposition probability is only 44% even for Pe = 0.0019. For a sufficient length of the pipe, the maximum value of the deposition probability is expected to approach unity as Lopez et al. have previously shown using an analogous approach in case of a longer domain for the parallel plate configuration [34]. When the number of the deposited particles reaches a critical value, the deposition probability drops sharply to rather low values indicating that any newly injected particles will have much less chance to deposit. This phenomenon is similar to the Random sequential Adsorption (RSA) process where the deposition kinetics becomes slow as the jamming limit is approached [39]. Furthermore, it is noteworthy that for all Péclet numbers, the overall deposition probability tends to decrease with N, and under our conditions, when N exceeds 15,000 all values of the deposition probability are less than 2% with only minor variations afterwards, indicating that the deposition process is almost over. Therefore, in this work, 2% was selected as the cut-off value for the injection process.

3.2. Spatial distribution of the density of the deposited particles

Since particles are considered to be volumeless before being adsorbed, the density distribution of the deposited particles, expressed as the number of deposited particles per unit area, is obviously isotropic in any x-y plane perpendicular to the pore symmetry axis. To show the influence of Pe on the axial (z-axis) variation of such a density, we will consider successively the tapered pipe geometry and the venturi-like geometry to highlight the difference between them. For the former, two Péclet numbers (0.0019 and 190) that are representative of diffusion dominant and advection dominant regimes were selected. For each Pe, the pore is divided into 15 slices along the z axis (the mean flow

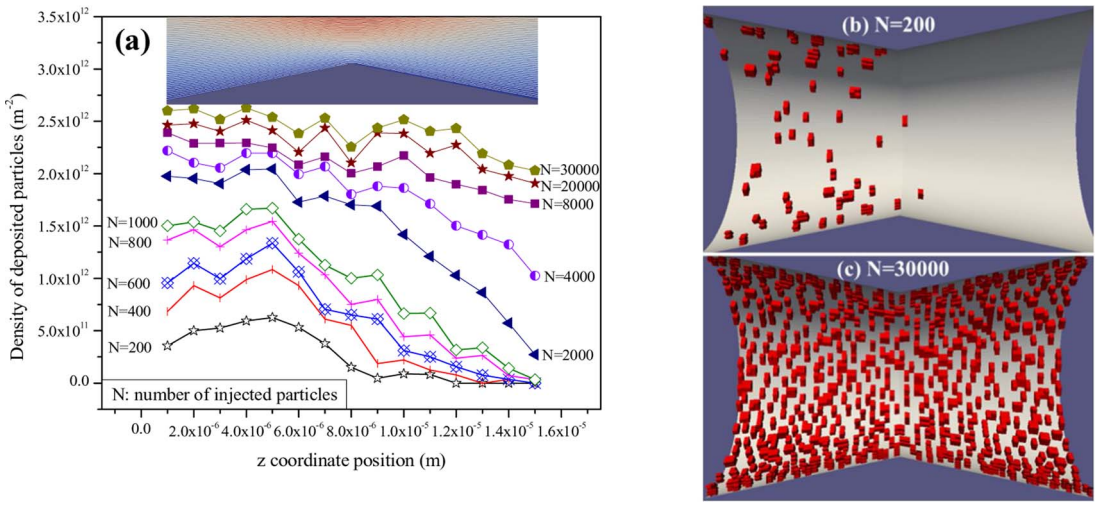

Fig. 4. (a) Spatial distribution of the density of deposited particles along the z coordinate at different N for Pe = 0.0019. (b) 3D sectional view of the tapered pipe at N = 200. (c) 3D sectional view of the tapered pipe at N = 30,000 (the flow occurs from left to right).

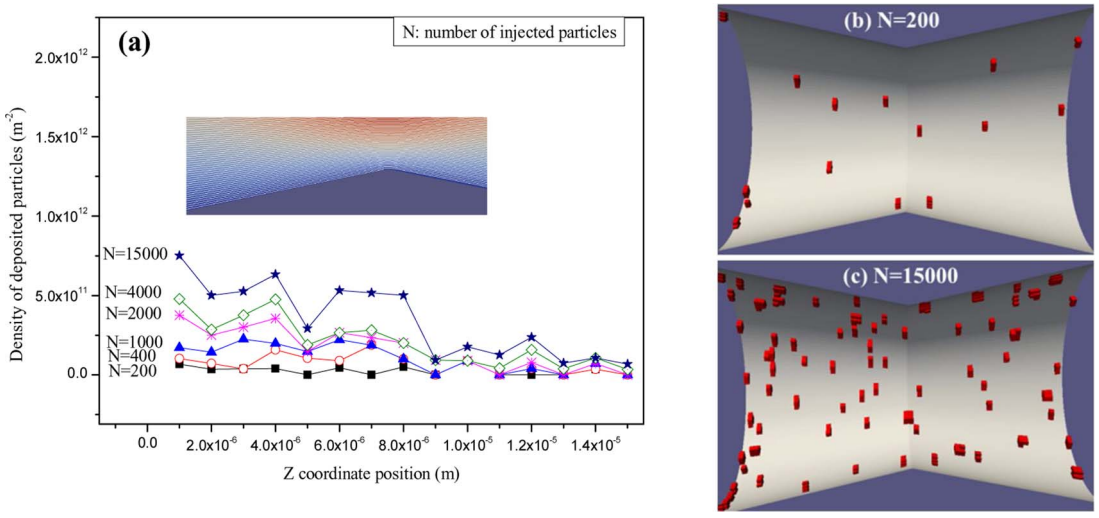

Fig. 5. (a) Spatial distribution of the density of deposited particles along the z coordinate at different N for Pe = 190. (b) 3D sectional view of the tapered pipe at N = 200. (c) 3D sectional view of the tapered pipe at N = 15,000 (Pe = 190, the flow occurred from left to right).

direction) and the density profile of the deposited particles is plotted for various numbers of injected particles, N (Figs. 4a and 5a).

For Pe = 0.0019, the deposition process is shown to be nearly piston-like. When N is small, the deposition distribution exhibits an apparent plateau near the inlet of the pipe, while the density remains small near the exit (Fig. 4b). By further increasing N, the density increase is more remarkable near the exit, where a large surface is still available for deposition, while it undergoes only a moderate change at the inlet zone. At later stages of deposition, a uniform deposit along the pipe is expected. Similar behavior was reported in the literature for column experiments when Polystyrene latex colloidal particles were injected into a synthetic consolidated porous medium and where deposition density was determined through local measurement of the attenuation of an incident gamma ray due to particles deposition [21,22]. Indeed, for low Pe the particle movement is mainly dominated by diffusion so that the velocity in the x-y plane may be higher than the velocity component in the mean flow direction. As a consequence, particles approach the surface wall and deposit first close to the inlet of the pipe. For high number of injected particles (over 2000) deposition at the inlet is almost over and the plateau value increases only slightly there approaching the jamming limit. Then, any further increase of injected particles mainly contributes to increase density in the rear part of the tube where free surface is still available for particles deposition leading to a uniform and dense deposit at the process end (Fig. 4a and c). This piston-like deposition was experimentally observed in column experiments [22] and the covering front displacement would be similar if the simulation domain was longer.

For Pe = 190, particle transport is dominated by advection, the spatial density distribution curves are nearly uniform along the pipe whatever the number of injected particles (Fig. 5a–c) leading to a scanty final deposit. This is a consequence of the high value of $\mathbf{V_{conv}}$ that greatly modify the excluded zone both in magnitude and shape. In this advection dominant regime, the restricted area in the rear of deposited particles is increased as flow velocity (or particle velocity here) increases resulting in a great impact of the hydrodynamic shadowing effect on pore surface covering. This phenomenon that is sometimes expressed in terms of the blocking factor was already experimentally evidenced [12,21,40,41] and was modelled [40,41] and numerically assessed [34]. Fig. 6a and b offer a clear view for Pe = 1.9 on how flow streamlines are modified in the vicinity of the wall due to particle deposition. It is then clearly seen that the original streamlines that were straight and parallel to the wall become highly deformed and peeled from the wall. Moreover and as the jamming ratio (ratio of characteristic size of the pore to that of the particle) is not too large, the

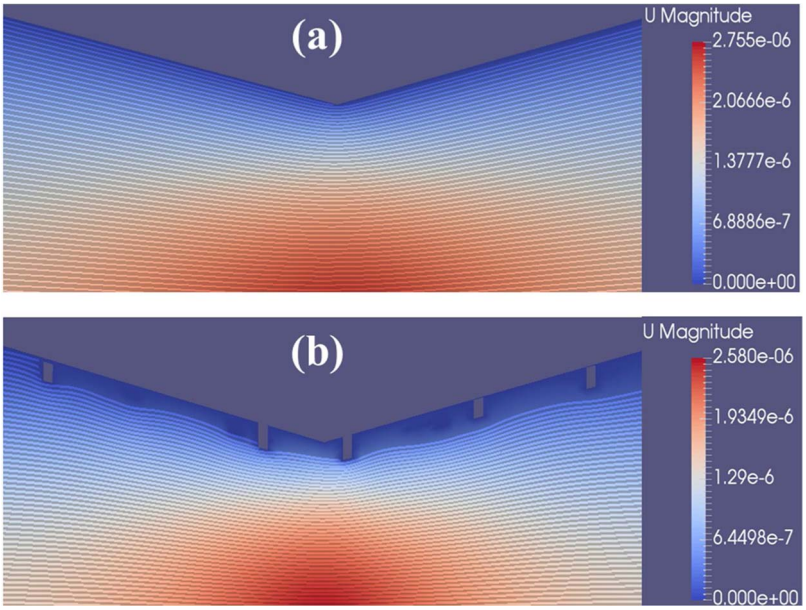

Fig. 6. Streamline profiles in the tapered pipe without (a) and with (b) deposited particles (Pe = 1.9).

streamlines become also squeezed decreasing the local Péclet number. Consequently, the capture efficiency decreases in a manner similar to that of an isolated spherical collector for which the capture efficiency of Brownian particles is predicted to vary as $Pe^{-2/3}$ [42].

Similarly, in case of venturi geometry, we studied the variation of the spatial distribution of deposit density with the number of injected particles along the pore axis and for a Pe interval that covers diffusion-dominant and advection-dominant regimes. In overall the observed behavior is similar to that observed for tapered pipe with the same features. However the existence of corners in this geometry may be seen to locally impact the density distribution. This is obvious in Fig. 7, corresponding to Pe = 0.0014, that shows a more or less deep minimum at each corner location corresponding to lower deposition.

Such a behavior may be attributed to the flow field in these zones since flow streamlines behave differently in this geometry. In Fig. 8, a net detachment of the streamlines at the corners is observed. These impede the particle deposition as locally flowing particles will tediously cross the critical distance for deposition. It must be noted that the asymmetry observed in Fig. 8 (between upstream and downstream) is due to the choice of equidistant points at the inlet face of the pipe for

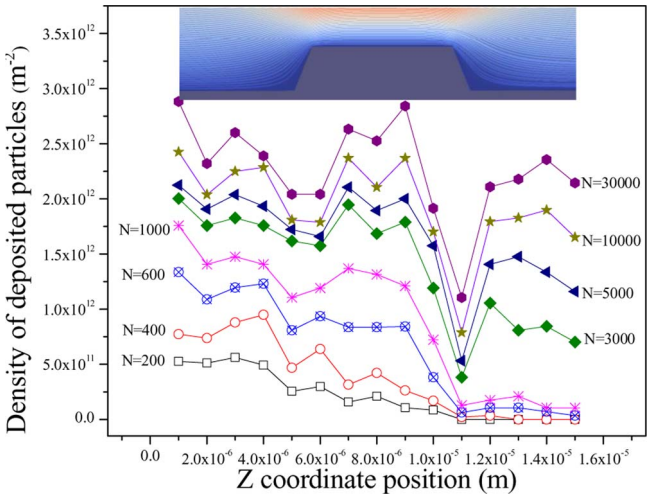

Fig. 7. Spatial distribution of the density of deposited particles along the z coordinate at different N for Pe = 0.0014.

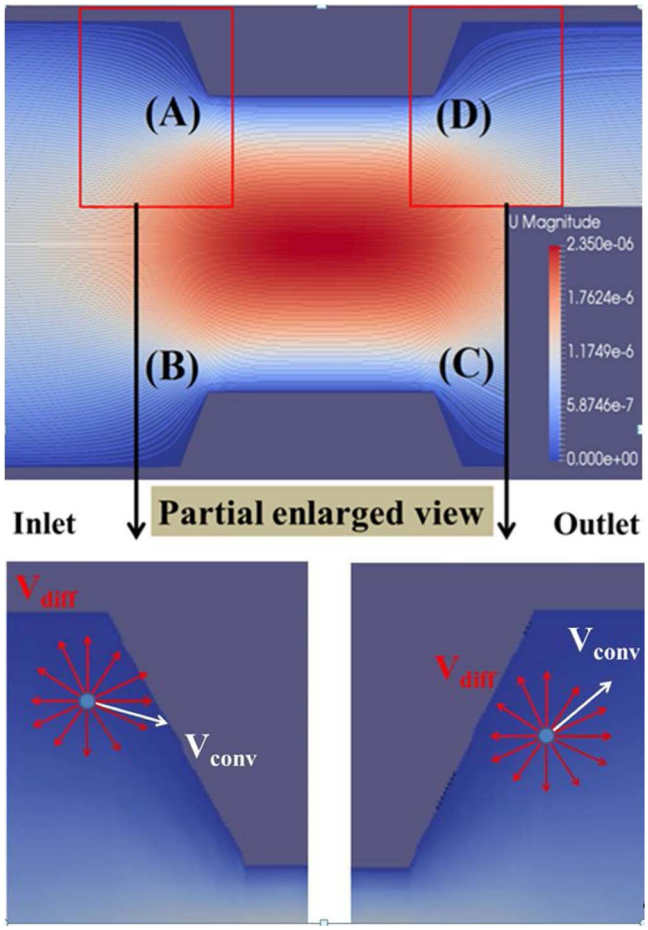

Fig. 8. Initial streamlines distribution in the venturi pipe at Pe = 1.4 and Re = 0.48×10^{-4} and an illustration of convective and diffusive components of the particle velocity near the corners.

plotting the streamlines. Moreover, the total particle velocity is composed of the convective and diffusive contributions presented as white and red arrows respectively in Fig. 8. As it can be seen, near the corner A, since the convective component of the velocity is pointing towards

the wall, a particle has a higher probability to come close to the wall and deposit. Near the corner D, the convective component of the velocity pushes the particle away from the wall and therefore, it has a lower probability to approach the wall and deposit. Same conditions apply in corners B and C. This behavior leads to a deposition probability in the second steep corners lower than the first steep corners as can be seen in Fig. 7.

Analogous behavior was observed at various Pe numbers even if the evaluation of the density of deposited particles is rather difficult at high Pe values due to less deposition as we emphasized before. However, one can expect additional hydrodynamic retention of Brownian particles in these zones when the Reynolds number is high due to flow recirculation. Such a retention mechanism was proven to be important in real porous media at grain-grain edges [26,32] and in cracks for rough pore surfaces [43].

Fig. 8. Initial streamlines distribution in the venturi pipe at Pe = 1.4 and Re = 0.48×10^{-4} and an illustration of convective and diffusive components of the particle velocity near the corners.

3.3. Variation of the dimensionless surface coverage

Surface coverage (Γ) is defined as the ratio of the total projection area of deposited particles to the total initial surface area of the pore surface before deposition. In this work, results are presented in terms of the dimensionless surface coverage Γ/Γ_{RSA}, where Γ_{RSA} was taken to be 0.546 [39] which corresponds to the value for pure diffusion regime and a flat surface using the Random Sequential Adsorption (RSA) model. The use of such a value is justified since the ratio of particle radius to pore surface curvature is low enough. The variation of Γ/Γ_{RSA} versus the number of injected particles (N) at Péclet numbers spanning from very low to very high values is plotted in Fig. 9 for the tapered pipe. It can be seen that, for all Pe values, Γ/Γ_{RSA} increases sharply with N in the early deposition stages and tends to a plateau value, $\Gamma_{final}/\Gamma_{RSA}$, that is of course reached for a smaller value of N for higher Pe. In the diffusion-dominant regime (for example, at Pe = 0.0019), $\Gamma_{final}/\Gamma_{RSA}$ is found to be close to that obtained in the same conditions for a straight capillary tube [44] and in parallel plates as well [34]. For Pe = 1900 where particle transport is mostly due to advection, $\Gamma_{final}/\Gamma_{RSA}$ is significantly reduced and is of only 0.08. It should be noted here that even at that extreme Pe values, the flow Reynolds number is low enough (< 0.1) and the flow may still be considered as creeping. Similar behavior was also observed in the case of the venturi geometry despite the existence of the corners with reduced deposition density therein affecting only slightly the value of $\Gamma_{final}/\Gamma_{RSA}$ (data not shown).

On Fig. 10, $\Gamma_{final}/\Gamma_{RSA}$ is plotted as a function of Pe for the two geometries considered here, for the capillary tube with constant cross

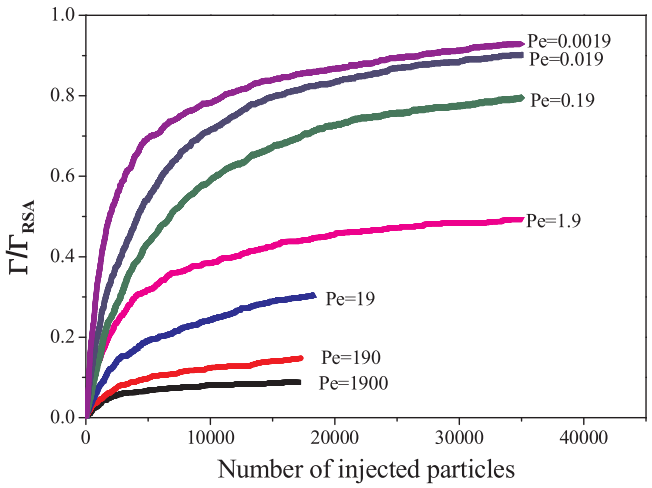

Fig. 9. Variation of dimensionless surface coverage Γ/Γ_{RSA} versus N at different Pe.

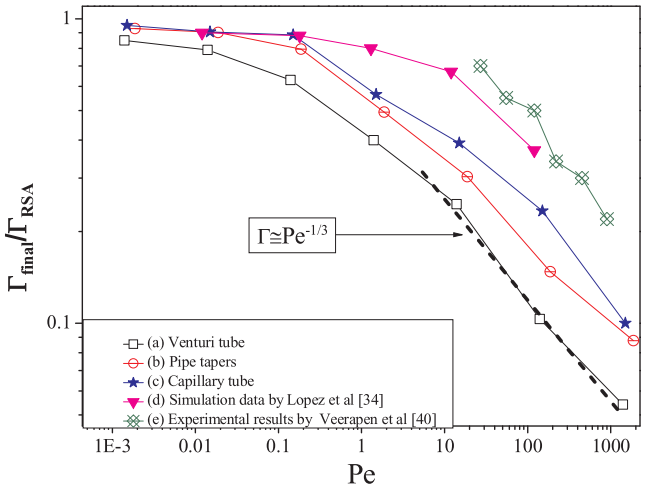

Fig. 10. Variation of $\Gamma_{final}/\Gamma_{RSA}$ versus Péclet number: (a) venturi tube; (b) tapered pipe; (c) capillary tube; (d) parallel planes of Lopez et al. [34]; (e) experimental results of Veerapen et al. [40].

section already investigated under the same conditions in a previous work [44], as well as the data obtained by Lopez and co-workers [34] from simulations performed for flow between parallel plates under comparable conditions. As we can see, as long as diffusion dominates, the surface coverage is close to Γ_{RSA} and is almost constant due to the high deposition probability in this regime and the precise form of the pore has a weak impact on the attained value of Γ_{final}. It is obvious that the upper limit of this regime varies from one geometry to another due to the values of $\bar{u}$ used for Pe calculation. After the diffusion dominant regime, a critical or transition zone is observed in which the Peclet number ranges approximately from 0.1 to 20 followed by an advection dominant regime. For this regime, $\Gamma_{final}/\Gamma_{RSA}$ decreases significantly with Pe. This is because the hydrodynamic shadowing effect comes to play and as mentioned before, particles are transported by the fluid over a distance increasing with the advection velocity until they may deposit downstream away from an already deposited particle, resulting hence in a lower surface coverage [12,21,34,40,41]. This finding is in qualitative agreement with experimental data that were already obtained by Veerapen and co-workers when sub-micrometric latex particles are injected through a non-consolidated silicon carbide porous medium [40]. Salehi [45] has developed a simple model that describes deposition of colloidal particles in advection-dominant regime and predicts the surface coverage for a flat surface to follow a power law as $\Gamma_{final} \cong Pe^{-1/3}$, which was shown to fit well the experimental data of Veerapen et al. [40].This power law is also drawn on Fig. 10 showing that despite the fact that the surface coverage in the venturi pipe leads to a satisfactory fit with such a trend, the agreement is less obvious when the other geometries are considered and more *in-silico* experiments at higher Péclet numbers are needed to draw any definite conclusion. Unni and Yang [18] have investigated colloids deposition in parallel channel by means of Brownian dynamic simulation by focusing on the variation of surface coverage with flow strength. They showed that Γ is a decreasing function of flow Reynolds number in a much more pronounced way but the considered range, from 20 to 60, was many orders of magnitude greater than in the present work.

4. Conclusions

The present study proposes a novel 3D-PTPO code (Three-Dimensional Particle Tracking model by Python® and OpenFOAM®) based on a Lagrangian method, to carry out microscale simulations of colloidal particle transport and deposition in converging/diverging capillaries (tapered pipe and venturi tube). The idea is to approach the behavior in porous media idealized as a bundle of capillaries with

variable cross sections. The main originality of the tool is to take into account the modification of the pore-space and therefore the flow field as particles are deposited on the pore-wall. Several main conclusions can be drawn: The probability for a particle to be deposited on the pore-wall surface is much higher when the transport is dominated by diffusion for the two geometries considered in this work. The deposited particle distribution along the pipes is piston-like for the diffusion-dominant regime, while the distribution is more uniform for the advection-dominant regime. Moreover, for all values of the Péclet number considered in this work ranging between 0.0019 and 1900, the dimensionless surface coverage Γ/Γ_{RSA} as a function of the number of injected particles (N) features a sharp increase in the early deposition stages and tends to a plateau value for higher N. The behavior of the final plateau corresponding to the maximum surface coverage $\Gamma_{final}/\Gamma_{RSA}$ as a function of Pe has been analyzed. For low Pe, a plateau could be observed for both geometries, the plateau value and the deposition kinetics are consistent with the random sequential adsorption (RSA) theory. At high Pe, the declining trends of $\Gamma_{final}/\Gamma_{RSA}$ versus Pe are in good agreement with the experimental and simulation results obtained by other studies. Finally, these results demonstrate that the numerical model could capture the physics of transport and deposition of colloidal particles in pores of simple geometry and could be used in further developments such as for transport in more complex geometries (unit cell of a sphere packing), multi-layer particle deposition, chemically patterned surfaces, etc.

Declarations of interest

None.

Acknowledgement

This work was supported in part by the China Scholarship Council (CSC) under the Grant CSC N° 201506260062.

References

[1] T. Tosco, J. Bosch, R.U. Meckenstock, R. Sethi, Transport of ferrihydrite nanoparticles in saturated porous media: role of ionic strength and flow rate, Environ. Sci. Technol. 46 (2012) 4008–4015.
[2] I.S. Ngene, R.G.H. Lammertink, M. Wessling, W.V.D. Meer, A microfluidic membrane chip for in situ fouling characterization, J. Membr. Sci. 346 (2010) 202–207.
[3] B. Asgharian, O.T. Price, W. Hofmann, Prediction of particle deposition in the human lung using realistic models of lung ventilation, J. Aerosol. Sci. 37 (2006) 1209–1221.
[4] B. Asgharian, W. Hofmann, R. Bergmann, Particle deposition in a multiple-path model of the human lung, Aerosol Sci. Technol. 34 (2001) 332–339.
[5] S. Bensaid, D.L. Marchisio, D. Fino, G. Saracco, V. Specchia, Modelling of diesel particulate filtration in wall-flow traps, Chem. Eng. J. 154 (2009) 211–218.
[6] S. Bensaid, D.L. Marchisio, D. Fino, Numerical simulation of soot filtration and combustion within diesel particulate filters, Chem. Eng. Sci. 65 (2010) 357–363.
[7] K.M. Yao, M.T. Habibian, C.R. O'Melia, water and waste water filtration: concepts and applications, Environ. Sci. Technol. 5 (1971) 1105–1112.
[8] S.A. Bradford, J. Simunek, M. Bettahar, M.T. van Genuchten, S.R. Yates, Modeling colloid attachment, straining, and exclusion in saturated porous media, Environ. Sci. Technol. 37 (2003) 2242–2250.
[9] P.R. Johnson, N. Sun, M. Elimelech, Colloid transport in geochemically heterogeneous porous media: modeling and measurements, Environ. Sci. Technol. 30 (1996) 3284–3293.
[10] N. Tufenkji, M. Elimelech, Correlation equation for predicting single-collector efficiency in physicochemical filtration in saturated porous media, Environ. Sci. Technol. 38 (2004) 529–536.
[11] D. Liu, P.R. Johnson, M. Elimelech, Colloid deposition dynamics in flow-through porous media: role of electrolyte concentration, Environ. Sci. Technol. 29 (1995) 2963–2973.
[12] C.H. Ko, M. Elimelech, The "Shadow effect" in colloid transport and deposition dynamics in granular porous media: measurements and mechanisms, Environ. Sci. Technol. 34 (2000) 3681–3689.
[13] C. Reeshav, Transport and Deposition of Particles onto Homogeneous and Chemically Heterogeneous Porous Media Geometries, Thesis, University of Alberta, 2011.
[14] C. Tien, Granular Filtration of Aerosols and Hydrosols, Butterworths, 1989.
[15] M. Elimelech, C.R. O'Melia, Effect of particle size on collision efficiency in the deposition of brownian particles with electrostatic energy barriers, Langmuir 6 (1990) 1153–1163.
[16] Z. Adamczyk, B. Siwek, K. Jaszczołt, P. Weronski, Deposition of latex particles at heterogeneous surfaces, Colloids Surf. A: Physicochem. Eng. Aspects 249 (2004) 95–98.
[17] T. Areepitak, J. Ren, Model simulations of particle aggregation effect on colloid exchange between streams and streambeds, Environ. Sci. Technol. 45 (2011) 5614–5621.
[18] H.N. Unni, C. Yang, Brownian dynamics simulation and experimental study of colloidal particle deposition in a microchannel flow, J. Colloid Interface Sci. 291 (2005) 28–36.
[19] Z. Adamczyk, M. Nattich, J. Barbasz, Deposition of colloid particles at heterogeneous and patterned surfaces, Adv. Colloid Interface Sci. 147–148 (2009) 2–17.
[20] V. Canseco, A. Djehiche, H. Bertin, A. Omari, Deposition and re-entrainment of model colloids in saturated consolidated porous media: experimental study, Colloids Surf. A Physicochem. Eng. Asp. 352 (2009) 5–11.
[21] D. Gharbi, H. Bertin, A. Omari, Use of gamma Ray attenuation technique to study colloid deposition in porous media, Exp. Fluids 37 (2004) 665–672.
[22] A. Djehiche, V. Canseco, A. Omari, H. Bertin, Experimental study of colloidal particles deposit in porous media: hydrodynamics and salinity effects, Comptes Rendus Mécanique 337 (2009) 682–692.
[23] A. Djehiche, M. Gafsi, V. Canseco, A. Omari, H. Bertin, Effet de la force Ionique et Hydrodynamique sur le Dépôt de Particules Colloïdales dans un Milieu Poreux Consolidé, Can. J. Chem. Eng. 93 (2015) 781–787.
[24] T. Baumann, C.J. Werth, Visualization of colloid transport through heterogeneous porous media using magnetic resonance imaging, Colloids Surf. A: Physicochem. Eng. Aspects 265 (2005) 2–10.
[25] R. May, Y. Li, The effects of particle size on the deposition of fluorescent nanoparticles in porous media: direct observation using laser scanning cytometry, Colloids Surfaces A: Physicochem. Eng. Aspects 418 (2013) 84–91.
[26] P. Klauth, R. Bauer, C. Ralfs, P. Ustohal, J. Vanderborght, H. Vereeken, E. Klumpp, Fluorescence macrophotography as a tool to visualize and quantify spatial distribution of deposited colloid tracers in porous media, Colloids Surf. A: Physicochem. Eng. Aspects 306 (2007) 118–125.
[27] W.P. Johnson, E. Pazmino, H. Ma, Direct observations of colloid retention in granular media in the presence of energy barriers, and implications for inferred mechanisms from direct observations, Water Res. 44 (2010) 1158–1169.
[28] S. Sasidharan, S. Torkzaban, S.A. Bradford, Coupled effects of hydrodynamic and solution chemistry on long-term nanoparticle transport and deposition in saturated porous media, Colloids Surf. A: Physicochem. Eng. Aspects 457 (2014) 169–179.
[29] S.R. Risbud, G. Drazer, Trajectory and distribution of suspended non-brownian particles moving past a fixed spherical or cylindrical obstacle, J. Fluid Mech. 714 (2013) 213–237.
[30] Y.-I. Chang, S.-C. Chen, E. Lee, Prediction of brownian particle deposition in porous media using the constricted tube model, J. Colloid Interface Sci. 266 (2003) 48–59.
[31] G. Boccardo, D.L. Marchisio, R. Sethi, Microscale simulation of particle deposition in porous media, J. Colloid Interface Sci. 417 (2014) 227–237.
[32] F.A. Coutelieris, M.E. Kainougiakis, A.K. Stubos, Low peclet mass transport in assemblages of spherical particles for two different adsorption mechanisms, J. Colloid Interface Sci. 264 (2003) 20–29.
[33] H. Gao, Q. Qiu, D. Fan, Y. Jin, L.-P. Wang, Three-dimensional microscale simulation and colloid transport in saturated soil porous media, Comput. Math. With Appl. 59 (2010) 2271–2289.
[34] P. Lopez, A. Omari, G. Chauveteau, Simulation of surface deposition of colloidal spheres under flow, Colloids Surf. A Physicochem. Eng. Aspects 240 (2004) 1–8.
[35] G. Malvault, A. Ahmadi, A. Omari, Numerical Simulation of Yield Stress Fluids Flow in Capillaries Bundle: Influence of the Form and the Axial Variation of the Cross-Section, (2016).
[36] Z. Adamczyk, B. Siwek, L. Czyk, Flow-induced surface blocking effects in adsorption of colloid particles, J. Colloid Interface Sci. 174 (1995) 130–141.
[37] P.R. Johnson, M. Elimelech, Dynamics of colloid deposition in porous media: blocking based on random sequential adsorption, Langmuir 11 (1995) 801–812.
[38] C.-H. Ko, S. Bhattacharjee, E. Elimelech, Coupled influence of colloidal and hydrodynamic interactions on the RSA dynamic blocking function for particle deposition onto spherical collectors, J. Colloid Interface Sci. 229 (2000) 547–567.
[39] J. Talbot, G. Tarjus, P.R.V. Tassel, From car parking to protein adsorption: an overview of sequential adsorption processes, Colloids Surf. A Physicochem. Eng. Aspects 165 (2000) 287–324.
[40] J.P. Veerapen, B. Nicot, G.A. Chauveteau, In-depth permeability damage by particle deposition at high flow rates, Paper Presented at European Conference on Formation Damage, The Hague (Netherlands), 21–22 May, 2001 SPE 68962.
[41] M.T.J. van Loenhout, E.S. Kooij, H. Wormeester, B. Poelsema, Hydrodynamic flow induced anisotropy in colloid adsorption, Colloids Surfaces A: Physicochem. Eng. Aspects 342 (2009) 46–52.
[42] V.G. Levich, Physicochemical Hydrodynamics, Prentice-Hall, 1962.
[43] N. Sefrioui, A. Ahmadi, A. Omari, H. Bertin, Numerical simulation of retention and release of colloids in porous media at the Pore scale, Colloids Surf. A Physicochem. Eng. Aspects. 427 (2013) 33–40.
[44] Y.J. Li, A. Omari, A. Ahmadi, H.T. Pu, Colloidal particle deposition in porous media under Flow:a numerical approach, Int. J. Model. Opt. 7 (2017) 43–47.
[45] N. Salehi, Mecanismes de Retention Hydrodynamique de Suspension Colloidales en Milieux Poreux Modeles, PhD Thesis, Orsay University, France, 1996.